Intercalation of Alkali Metal in WS_2 Nanoparticles, Revisited

F. Kopnov,[†] Y. Feldman,[‡] R. Popovitz-Biro,[‡] A. Vilan,[‡] H. Cohen,[‡] A. Zak,[§] and R. Tenne*,[†]

Department of Materials and Interfaces and Chemical Research Support Unit, Weizmann Institute, Rehovot 76100, Israel, and "NanoMaterials", Ltd., Weizmann Science Park, Building 18, 18 Einstein Street, P.O. Box 4088, Nes-Ziona 74140, Israel

Received January 3, 2008. Revised Manuscript Received February 17, 2008

WS_2 inorganic fullerene-like (IF) nanoparticles were subjected to intercalation with potassium, sodium, and rubidium atoms in heated sealed ampules. The product of the intercalation process was not pure and was composed of both intercalated and nonintercalated phases. X-ray diffraction measurements under inert conditions of the intercalated powders showed that the interlayer expansion was correlated with the alkali metal radius. Small increase of the *a*-axis was observed as well and was explained on the grounds of the WS_2 band structure. The XPS analysis of the rubidium intercalated material showed a rise in the Fermi energy as a result of the intercalation, endowing the originally p-type nanoparticles an n-type character.

Introduction

WS_2 belongs to the class of layered-type transition metal dichalcogenide (TMDCs) compounds whose crystal structure results from the stacking of sheets of hexagonally packed atoms in the sequence S−W−S//S−W−S. The tungsten atom is bonded to six sulfur atoms in a trigonal prismatic coordination within each S−W−S molecular layer. This unique structure allows accommodating (intercalation) atoms, ions, or organic molecules in the van der Waals gap between the weakly bonded S−W−S layers. Partial or even complete charge transfer from the guest atoms to the host matrix serves as the stabilizing factor in this process. The changes in the structural and electronic properties of the host accompanied with the intercalation have led to much attention in these intercalation compounds for the past 40 years.[1] The alkali metals Li, Na, K, Rb, Cs and also simple metals such as Ag and Cu readily enter between the layers of TMDCs to form intercalated complexes. Special attention has been paid to the Li/MoS_2 and Li/TiS_2 systems since they are used in some of the lithium based rechargeable batteries.[2] A number of experimental methods to achieve intercalation of metal as well as organic moieties have been described in the literature.[1] Diffraction studies of the intercalated TMDCs revealed a variety of interesting structural changes in the host material. The layer separation in general is found to increase from typically 5−10% for metal intercalates up to a factor of 10 for large organic molecules.[3] There can also be small but measurable changes in the bond lengths within the host lattice itself. Thus, extended X-ray absorption fine structure (EXAFS) experiments by Bourdillon et al.[4] on $Rb_{0.28}NbSe_2$ have shown that within the $NbSe_2$ layers, the Nb−Nb distance (*a*-axis) expands by 0.013 Å, while the Nb−Se distance remains unchanged. It follows that in this case the Se−Nb−Se sandwich flattens without altering the Nb−Se bond length. In contrast to the pristine layered metal-dichalcogenides, the alkali−metal intercalation compounds are highly reactive products. They are all sensitive to moisture, some of them are even pyrophoric, and they must be kept in an inert atmosphere. The hydrated products can be obtained by a direct reaction of the alkali intercalates with moisture,[5] through a reaction of the host chalcogenides with aqueous solution of the alkali-metal hydroxides[6] or electrochemically by the electrolysis of aqueous solutions at the chalcogenide cathode.[7] In all of these cases an increase in the *c*-axis was observed. It has been possible to interpret many of the changes in the optical and electrical properties of alkali metal intercalated TMDCs in terms of the "rigid band" model. Within this model the host material band structure is unaltered by the presence of the intercalant (guest atom) except for increased filling of the transition metal d band. This model is generally limited to no more than 10% of metal intercalation. It is believed that the guest−host charge transfer is the driving force toward intercalation. Thus optical studies of Na_xMoS_2 demonstrated the disappearance of the A and B exciton levels with increasing *x* due to Thomas−Fermi screening by the free carriers. Electrical transport measurements revealed that MoS_2 became metallic after potassium intercalation.[8] Furthermore, a semiconductor to metal transition induced by K intercalation into WS_2 in ultra-high

[†] Department of Materials and Interfaces, Weizmann Institute.
[‡] Chemical Research Support Unit, Weizmann Institute.
[§] "NanoMaterials", Ltd.

(1) Friend, R. H.; Yoffe, A. D. *Adv. Phys.* **1987**, *36*, 1.
(2) Benavente, E.; Gonzalez, G. Mater. *Res. Bull.* **1997**, *32*, 709.
(3) Legrand, A. P.; Flandrois, S. North Atlantic Treaty Organization. Scientific Affairs Division. *Chemical physics of intercalation*; Plenum: New York, 1987.
(4) Bourdillon, A. J.; Pettifer, R. F.; Marseglia, E. A. *Physica B & C* **1980**, *99*, 6.
(5) Wiegers, G. A.; Vanderme, R; Vanheini, H; Klooster, Hj; Alberink, A. J. *Mater. Res. Bull.* **1974**, *9*, 1261.
(6) Whitting, M. S. *Mater. Res. Bull.* **1974**, *9*, 1681.
(7) Schollho, R; Meyer, H. *Mater. Res. Bull.* **1974**, *9*, 1237.
(8) Hermann, A. M.; Somoano, R.; Hadek, V.; Rembaum, A. *Solid State Commun.* **1973**, *13*, 1065.

10.1021/cm800020p CCC: $40.75
Published on Web 05/21/2008

vacuum was observed by X-ray photoelectron spectroscopy and other techniques.[9]

Since the first inorganic fullerenes-like (IF) structures and nanotubes were synthesized much work has been invested in developing new preparation routes of these nanostructures and studying their growth mechanisms.[10] For example, recent studies report on the synthesis of WS_2 hollow nanoparticles via metal−organic chemical vapor deposition[11] starting from $W(CO)_6$ and elemental sulfur. Moreover, chemical nanofabrication can be used as well to produce patterned and free-standing TMDCs nanostructures out of different metals and different chalcogens.[12] Furthermore, some chemical and physical properties of these nanomaterials have been extensively studied.[13,14] Attention has been paid to using inorganic nanotubes as lithium and hydrogen storage media.[15] Thus, TiS_2[16] and protonated titanate and titania nanotubes[17] were successfully intercalated with lithium. In the case of lithium intercalated TiS_2 nanotubes expansion of the interlayer (the *c*-axis) distance was observed.[16] Magnetic measurements of sodium and potassium intercalated IF-MS_2 (M = Mo, W) nanoparticles[18] indicated a diamagnetic to paramagnetic transition after the intercalation. Recent studies of lithium doped MoS_2 nanowires[19] revealed that these structures showed a very large, nearly temperature-independent Pauli-like susceptibility.

In the course of the present work IF and 2H-WS_2 (2H stands for a hexagonal unit cell consisting of two layers) powders were intercalated with sodium, potassium and rubidium by subjecting the relevant powder to the metal vapors at elevated temperatures. Special measures were taken to keep airtight and humidity free atmosphere during the intercalation and the analyses of the materials. This point distinguishes the present study from our previous work, where air tightness was, most likely, not adequate, especially during the transfer of the samples from the quartz ampules to the various measurements.[18] Furthermore, intercalation of IF nanostructures with rubidium, which is reported here, was not studied before. The X-ray diffraction (XRD) analysis showed a clear correlation between the *c*-axis expansion of the host and the radius of the intercalating atom. Moreover, a small but discernible increase in the *a*-axis values of the intercalated species was found as compared to the pristine IF nanoparticles. The X-ray photoelectron spectroscopy (XPS) study of the rubidium intercalated IF powder established a rise of the Fermi energy which provided evidence for the guest−host charge transfer.

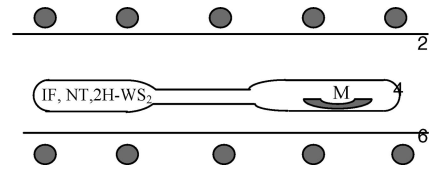

Figure 1. Schematic drawing of an experimental setup for the intercalation.

Table 1. Temperature Gradients and Time Duration of the Intercalation Processes for IF and 2H-WS_2 Powders

metal	temperature gradient T_1(powder)/T_2(metal) (°C)	time of the intercalation process (days)
Na	415/440	21
K	290/325	12
Rb	480/505	21

Experimental Section

The intercalation process was carried out by a two-zone vapor transport technique. IF (diameter of 60−120 nm) nanoparticles and 2H-WS_2 (1−10 μm width, around 0.5 μm thickness; Alfa Aesar) powders were used in this study. They were inserted into a two section Pyrex/quartz ampule (Figure 1) together with alkali metal (Na, K, Rb) to provide a spatial separation between the metal and the powder. To prevent a direct contact between the alkali metal and the glass/quartz, the metal was loaded into a molybdenum container, which was placed in the quartz ampule containing the WS_2 powder. The ampule was evacuated for 2−3 h under vacuum of 10^{-5} Torr and then sealed and placed inside a two zone furnace which maintained the temperature gradient. The alkali metal was held at a temperature that provided metal vapor pressure of 10^{-1} Torr, while the IF or 2H powder was situated at the colder zone of the temperature gradient. The ampules were left for 2−3 weeks inside the furnace. Table 1 describes the temperature gradients and intercalation times for the three kinds of alkali metals. After the intercalation reaction was stopped, the ampule was cooled down to room temperature. Numerous intercalation experiments were performed with different time durations. The data shown in Table 1 seem to represent an equilibrium state between the alkali metal vapors and the host. The intercalated material was analyzed by X-ray diffraction (XRD), TTRAX-III Rigaku; transmission electron spectroscopy (TEM), TEM CM-120 Philips equipped with energy dispersive spectrometer (EDS)-EDAX model Phoenix; and TEM Technai F30 furnished with Gatan imaging filter enabling electron energy loss spectroscopy (EELS). X-ray photoelectron spectroscopy (XPS) was done by Kratos AXIS-HS analytical system using a monochromatized Al Kα (1486.6 eV) source. The XRD patterns were analyzed with Jade 8 software. To prevent exposure of the material to the ambient atmosphere during the diffraction experiments the prepared powder was rapidly loaded into a quartz capillary and sealed with the vacuum sealant inside the glovebox with argon atmosphere. To prevent the exposure of the sample to the atmosphere during preparation for XPS studies, a special glovebox was mounted on the air lock of the XPS instrument. The powder sample in the airtight vile was placed inside the glovebox. The glovebox was purged and flushed with dry nitrogen prior to opening the vile with the sample. To reduce exposure of the sample to air prior to the TEM analyses, the powder was dispersed in dry

(9) Ohuchi, F. S.; Jaegermann, W.; Pettenkofer, C.; Parkinson, B. A. *Langmuir* **1989**, *5*, 439.
(10) Remskar, M. *Adv. Mater.* **2004**, *16*, 1497.
(11) Zink, N.; Pansiot, J.; Kieffer, J.; Therese, H. A.; Panthöfer, M.; Rocker, F.; Kolb, U.; Tremel, W. *Chem. Mater.* **2007**, *19*, 6391.
(12) Stender, C. L.; Odom, T. W. *J. Mater. Chem.* **2007**, *17*, 1866.
(13) Golberg, D.; Bando, Y.; Tang, C. C.; Zhi, C. Y. *Adv. Mater.* **2007**, *19*, 2413.
(14) Li, Q.; Walter, E. C.; vanderVeer, W. E.; Murray, B. J.; Newberg, J. T.; Bohannan, E. W.; Switzer, J. A.; Hemminger, J. C.; Penner, R. M. *J. Phys. Chem. B* **2005**, *109*, 3169.
(15) Cheng, F. Y.; Chen, J. *J. Mater. Res.* **2006**, *21*, 2744.
(16) Chen, J.; Tho, Z. L.; Li, S. L. *Angew. Chem., Int. Ed.* **2003**, *42*, 2147.
(17) Zhang, H.; Li, G. R.; An, L. P.; Yan, T. Y.; Gao, X. P.; Zhu, H. Y. *J. Phys. Chem. C* **2007**, *111*, 6143.
(18) Zak, A.; Feldman, Y.; Lyakhovitskaya, V.; Leitus, G.; Popovitz-Biro, R.; Wachtel, E.; Cohen, H.; Reich, S.; Tenne, R. *J. Am. Chem. Soc.* **2002**, *124*, 4747.
(19) Jaglicic, Z.; Jeromen, A.; Trontelj, Z.; Mihailovic, D.; Arcon, D.; Remskar, M.; Mrzel, A.; Dominko, R.; Gaberscek, M.; Martinez-Agudo, J. M.; Gomez-Garcia, C. J.; Coronado, E. *Polyhedron* **2003**, *22*, 2293.

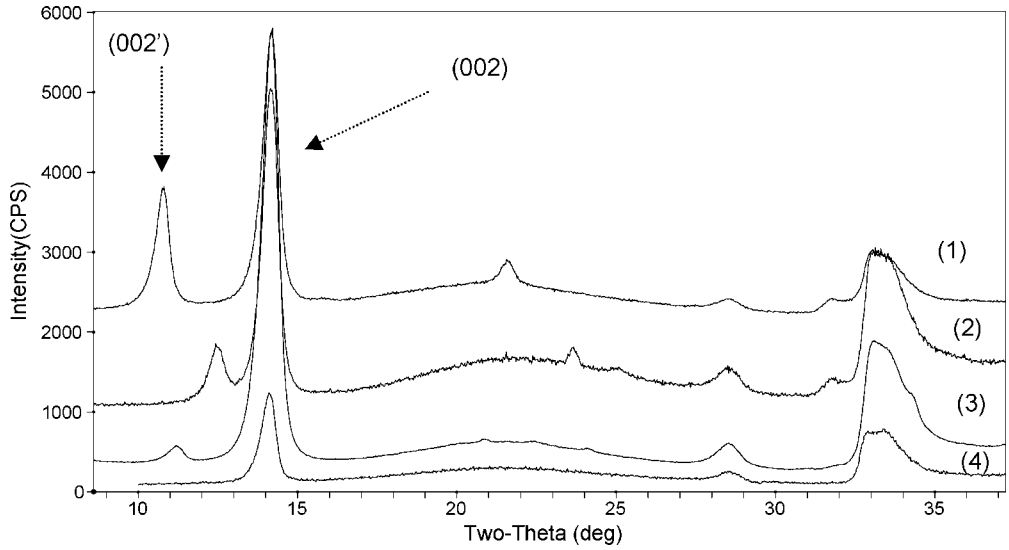

Figure 2. XRD patterns of rubidium (1), sodium (2) and potassium (3) intercalated IF and pristine IF (4).

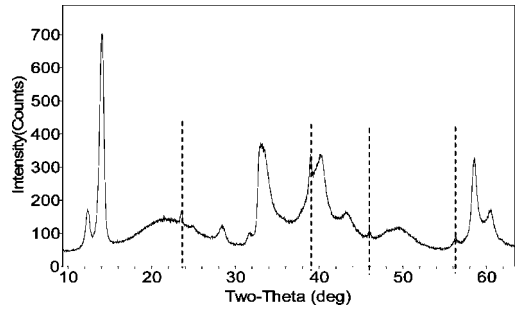

Figure 3. XRD pattern of sodium intercalated IF-WS_2 powder; the Na_2S peaks are designated by the dashed lines.

ethanol shortly after taking the sample out of the dry box and immediately inserted inside the microscope.

Results and Discussion

X-ray Powder Diffraction Analysis. The IF and 2H-WS_2 powders underwent intercalation reaction with sodium, potassium, and rubidium. X-ray diffraction measurements of the intercalated powders under inert conditions indicated the presence of several phases. The *c*-axis expansion served as evidence that the intercalant atoms were admitted inside the van der Waals gap of the WS_2 structure of the nanoparticles.[20] The existence of the (002′) and (002) peaks demonstrated that the product was not homogeneous and was composed of both intercalated and nonintercalated phases (Figure 2). The intercalated phase consisted of IF or 2H-WS_2 particles with the alkali atoms inserted in the van der Waals gap between the layers. The nonintercalated phase consisted of 2H or IF-WS_2 particles which were not affected by the alkali atoms and remained intact during the intercalation process. Additionally sodium sulfide Na_2S was formed in the course of the reaction of IF-WS_2 with sodium (Figure 3). A mixture of K_2S_4 and K_2S_6 phases appeared in the course of intercalation of 2H-WS_2 with potassium. Furthermore, weak peaks which could be associated with potassium sulfide compounds were identified in the XRD pattern of the potassium intercalated IF-WS_2 powder. The peak intensities corresponding to the K_2S_4, K_2S_6, and K_2S phases were found to be at the noise level. These findings may indicate that an unwieldy excess of potassium (sodium) was added to the ampule. The van der Waals gap expansion of the intercalated phase was observed to depend on the radius of the alkali atom: as expected the greatest interlayer expansion was obtained for the rubidium intercalation and the least for the intercalation with sodium atoms, Table 2. These results are profoundly different from the previous intercalation study[18] where the *c*-axis expansion of the sodium and potassium intercalated IF-WS_2 nanoparticles was found to swell up to 18.96 Å. That increase in the *c*-axis value was attributed to the insertion of water molecules inside the van der Waals gap. In that study the intercalated powder was exposed to the ambient during the XRD measurements, which could result in substantial intake of water by the alkali atom guests. The driving force for the water insertion into the lattice is the hydration of the intercalated alkali atoms.

Table 2. Comparison of the *c* Parameter of the Intercalated and Nonintercalated Phases

material	IF-WS_2 *c*-axis (±0.01) (Å)	2H-WS_2 *c*-axis (±0.01) (Å)
pristine material	12.49	12.36
Na intercalated	14.36	14.32
K intercalated	16.07	15.89
Rb intercalated	16.71	16.59
Rb_xIF after 3 months of storage	18.62	
Rb_xIF_a[a]	17.41	

[a] Synthesis where Rb grains mixed with IF.

The area under the (002) and (002′) peaks allows estimating the atomic percentage of the intercalated phase (note that this percentage does not represent the amount of the loaded alkali metal). Quite surprisingly, the IF powder contained more of the intercalated phase than the 2H-WS_2 material, under similar conditions. This finding is again in conflict with the previous data,[18] where the 2H polytype was found to have higher loading of the intercalant than the IF nanoparticles. This discrepancy can be probably attributed to the improved dryness control of the present system as

(20) Somoano, R. B.; Hadek, V.; Rembaum, A. *J. Chem. Phys.* **1973**, *58*, 697.

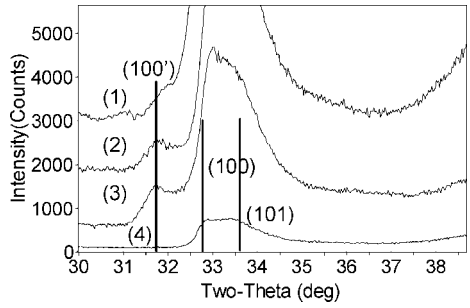

Figure 4. XRD patterns of potassium (1), sodium (2), and rubidium (3) intercalated IF and pristine IF (4); (100′), (100), and (101) peaks are designated.

Table 3. Highest Atomic Percentage of the Intercalated Phase that Was Observed

	IF intercalated phase %	2H intercalated phase %
Na	12	0.3
K	6.3	3.4
Rb	39	3.6

Table 4. Comparison of the (in-plane) *a*-Axis Values in the Intercalated and Nonintercalated Phases

material	IF-WS_2 *a*-axis (±0.002) (Å)	2H-WS_2 *a*-axis (±0.002) (Å)
pristine material	3.16	3.16
Na intercalated	3.26	
K intercalated	3.25	3.25
Rb intercalated	3.27	3.29
Rb_xIF after 3 months of storage	3.24	
Rb_xIF_a[a]	3.25	

[a] Synthesis where Rb grains were mixed with IF.

compared to the previous study.[18] Furthermore, the amount of the intercalated phases in the reacted powders of both IF and 2H-WS_2 depended on the specific alkali metal. The highest percentage of the intercalated phase for both kinds of powders was observed after the reaction with rubidium. The lowest percentage was obtained with sodium for the 2H-WS_2 material, whereas in the case of the IF powder, the reaction with potassium gave the lowest amount (atomic percentage) of the intercalated phase. Furthermore, the fraction of the intercalated IF phase was higher than the amount of the intercalated 2H-WS_2 phase with the same metal under the same conditions. This observation may be attributed to the difference in the surface to volume ratio of the two kinds of particles, which is greater by more than an order of magnitude for the IF nanoparticles. This result may also indicate that the system has not reached a complete equilibrium state even after 3 weeks of the intercalation reaction. Table 3 summarizes the experimental observations.

Besides the (002′) peak the XRD patterns of the intercalated IF and 2H-WS_2 powders demonstrated an additional peak (100′) next to the position of the (100) peak of the IF-WS_2 and 2H-WS_2 phases (Figure 4). The sodium intercalated 2H-WS_2 powder constituted the exception, since such a peak was not observed there, probably due to the low degree of sodium intercalation. This peak corresponds to an increase of 0.11−0.13 Å in the *a*-axis value in the intercalated phase. The calculated values of the expanded *a* parameter are presented in Table 4. Moreover, the XRD pattern of the

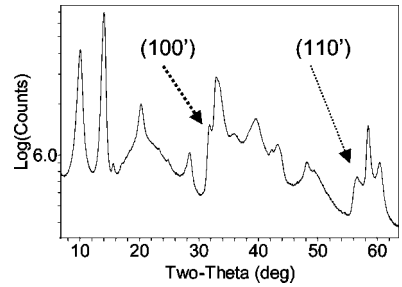

Figure 5. Rubidium intercalated IF-WS_2; the additional (100′) and (110′) peaks are assigned

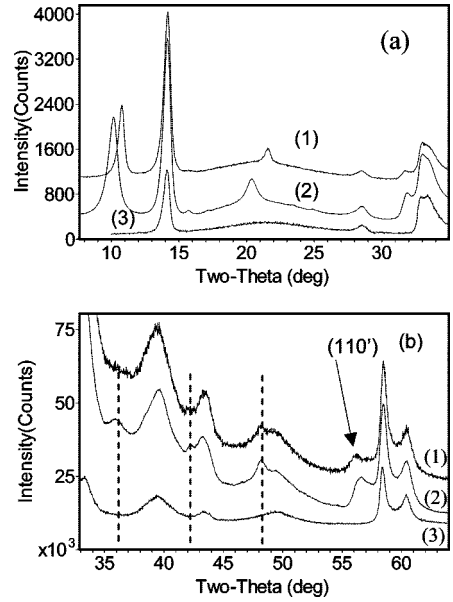

Figure 6. (a and b) The XRD patterns of the IF-WS_2 powder, Rb_xIF (1), Rb_xIF_a (2), and pristine IF (3). The unidentified lines are designated by dashed lines.

rubidium intercalated IF powder (Figure 5) demonstrated a peak that was identified as (110′). Both the (100′) and (110′) lines of the rubidium intercalated compound yielded an expanded *a*-axis (3.27 Å), Table 4, compared to the pristine phase (3.16 Å).

As was mentioned in the experimental part, the metals and the IF powder were kept in separate parts of the ampule during the synthesis. However, in some cases several grains of rubidium mixed accidentally with the IF powder, and the intercalation process was left to proceed. In these cases the positions of the intercalation peaks were slightly shifted compared to the corresponding lines of the intercalated material which was produced in the reaction where the metal and the powder were kept separately. Figure 6a,b shows the XRD pattern of the material from the synthesis where the rubidium grains had mixed with the IF powder Rb_xIF_a: the (002′) peak was further shifted to lower angles and gave the *c*-axis value of 17.41 Å instead of the usual value of Rb intercalated IF-WS_2 (16.71 Å); see Table 2. The difference in the *c*-axis increase in the two cases can be probably attributed to the different interactions between the rubidium atoms and the host. A similar phenomenon was not observed in the case of potassium intercalation. Moreover, the Rb_xIF_a XRD pattern shows that the (100′) and (110′) peaks also moved, however, in opposite direction to that of the (002′) line. The

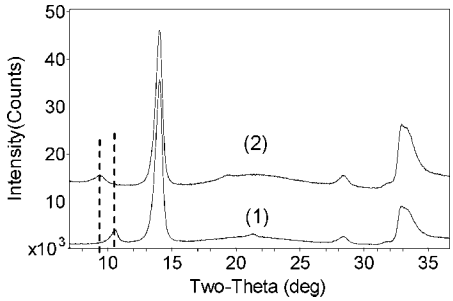

Figure 7. XRD patterns of the freshly intercalated powder (1) and of the same powder after three months of storage (2). The (002′) peaks are marked by dashed lines.

a-axis value of the intercalated phase in the Rb_xIF_a was found to be 3.25 Å rather than 3.27 Å for the regularly intercalated IF-WS_2 phase (see Table 4).

Furthermore, Figure 7 compares two XRD patterns of another rubidium intercalated IF powder. One of the patterns was obtained on a freshly prepared powder, while the other was obtained on that sample after 3 months of storage time (in the glovebox) during which the material had absorbed some water. It was found that in this case the *c*-axis of the intercalated phase had expanded from 16.71 Å up to 18.62 Å, whereas the *a*-axis had shrank to 3.24 Å compared with 3.27 Å for the freshly intercalated phase. It can be seen that both depicted cases (rubidium intercalated IF powders after 3 months of storage and when the metal grains and IF nanoparticles had mixed) showed the same tendency; that is, when the (002′) line of the intercalated phase moved to lower angles, i.e., to larger interlayer spacing, the (100′) and (110′) peaks, characterizing the *a*-parameter, shifted to higher angles from their initial values, respectively, Tables 2 and 4. Note, however, that in both cases the *a*-parameter is increased compared with the pristine IF-WS_2 material (3.16 Å). Increase in the *a*-parameter upon intercalation can be explained considering the band structure of WS_2. The top of the valence band of WS_2 contains d_{z^2}[21] orbitals and chalcogen p states while the conduction band is derived from the non bonding d_{xy} and $d_{x^2-y^2}$ orbitals.[9] Previous studies[22] showed that the pristine IF material was a p-type semiconductor. It might be assumed that upon intercalation electrons are transferred from the rubidium atoms to the empty states in the conduction band. Consequently, the electron density increases within the plane of the metal atoms and between coplanar S atoms and this phenomenon leads to the repulsion between adjacent sulfur or tungsten atoms (Figure 8).[4] The increased electron density in the plane leads to a repulsion between tungsten atoms and between sulfur atoms as well.[4] The experimental results presented above show that while the interlayer distances grew by 1.91 Å due to the water absorption, the expanded *a*-parameter was reduced only by 0.03 Å compared to the freshly intercalated sample, Tables 2 and 4. Probably some charge transfer to the water molecules occurred leading to a reduced charge density at the W atom and consequently reduction in the *a*-parameter.

(21) Ito, T.; Iwami, M.; Hiraki, A. *J. Phys. Soc. Jpn.* **1981**, *50*, 106.
(22) Kopnov, F.; Yoffe, A.; Leitus, G.; Tenne, R. *Phys. Status Solidi B* **2006**, *243*, 1229.

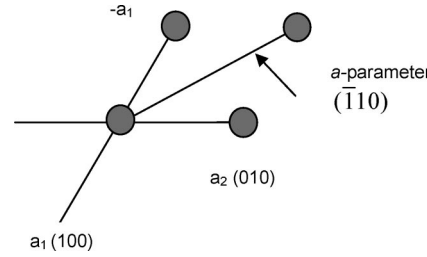

Figure 8. In-plane crystal directions in 2H-WS_2; solid circles represent either metal or chalcogen atoms.

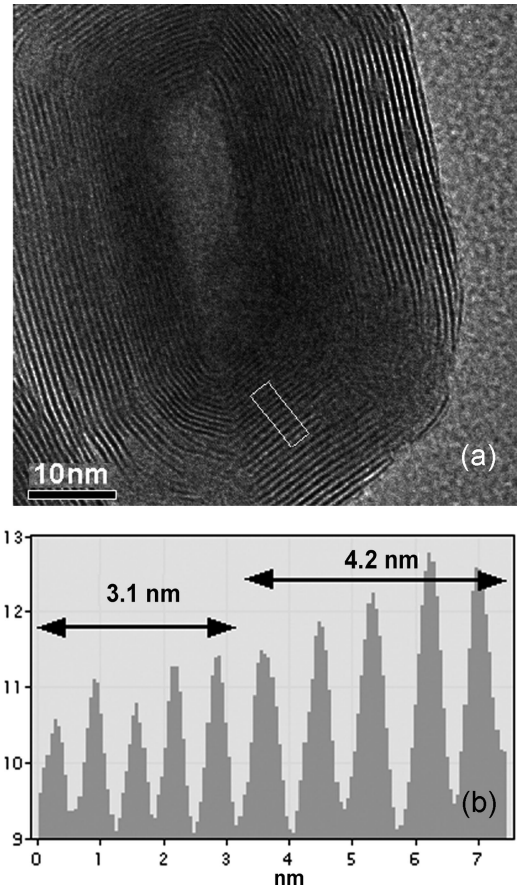

Figure 9. (a) TEM image of a typical rubidium intercalated IF particle and (b) the intensity profile of the framed layers at the interface between the pristine (inner) and the intercalated (outer) lattices. The difference between the outermost WS_2 layers (Rb intercalated) and the unmodified inner layers is clear.

Another interesting observation was the presence of the unidentified peaks in the pattern of the rubidium intercalated IF powder (Figure 6b). These lines were observed in the two cases where the percentage of the intercalated phase was the highest. Further experiments are needed for a complete assignment of these peaks.

TEM and Electron Energy Loss Spectroscopy (EELS)/ TEM Analysis. High Resolution TEM analysis was done for the rubidium intercalated phase, since this metal gives the greatest layer expansion and the Z-contrast between the host and the guest is the highest. Furthermore, the Rb-intercalated IF phase was not studied before. As can be seen in Figure 9 the outermost layers of the closed IF nanostructures expanded significantly suggesting that they underwent intercalation, whereas the inner layers of the closed IF

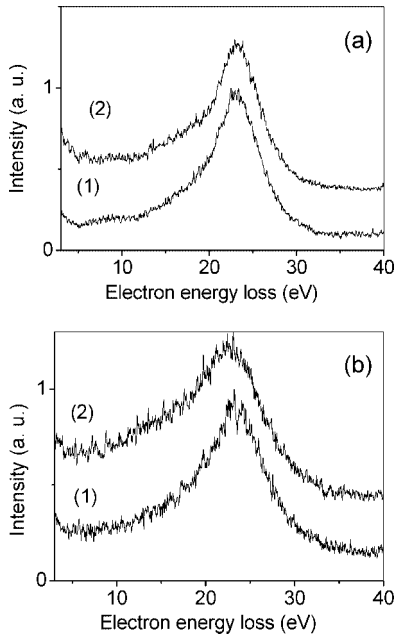

Figure 10. Typical electron energy loss spectra of (a) a pristine IF nanoparticle, (1) the whole particle and (2) the edge of the nanoparticle, and (b) a Rb intercalated IF particle, (1) the whole particle and (2) the edge of the particle.

Table 5. Width at Half Maximum of the EELS Spectra

type of the material	fwhm of the whole particle	fwhm of the edge of the particle
IF pristine	6.5 (±0.3) eV	9.0 (±0.5) eV
Rb intercalated IF particle	7 (±0.3) eV	11 (±0.5) eV

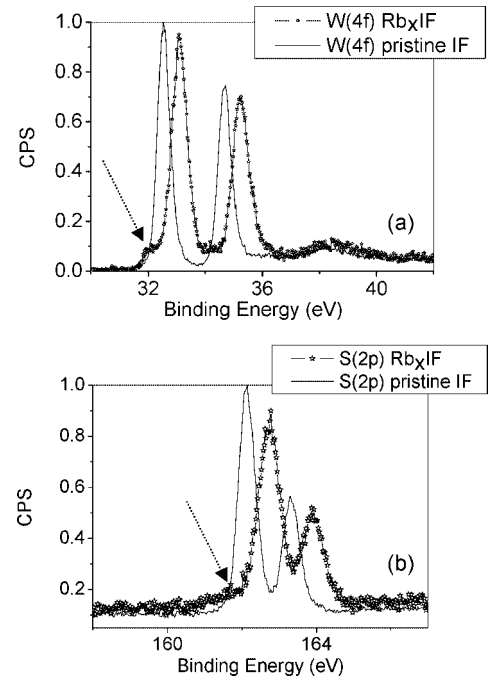

Figure 11. XPS windows of rubidium intercalated and pristine IF powder: (a) W(4f), (b) S(2p). Arrow points to the shoulder in each spectrum.

Table 6. Energy Band Shifts $E_{intercalated}-E_{pristine}$ of the Rb Intercalated Compared with the Pristine IF-WS_2 Phase

band	W(4f)	S(2p)	valence band (VB) shift	VB threshold shift
energy shift (mV)	572 (±50)	600 (±50)	600 (±50)	200 (±50)

nanostructures remained intact. One can propose that the alkali metal atoms diffuse from the outer surface of the particle along the defects into the inner layers. Intensity profile analysis shows that the distance between the outer expanded layers is 8.4 Å and between the intact inner layers is 6.2 Å, which is in good agreement with the XRD analysis. Obviously, the interlayer expansion due to the intercalation of the closed layers leads to a significant accumulation of strain in the IF nanoparticle. The deeper the penetration of the alkali atom into the core of the IF nanoparticle, the larger the accumulated strain. This strain acts against the chemical driving force for the intercalation until an equilibrium state is attained. Unfortunately, EDS and EELS/TEM analyses of rubidium intercalated nanoparticles are practically impossible, due to the overlap between the rubidium and tungsten lines.

The low loss EELS region of the rubidium intercalated and pristine IF particles showed slight differences (Figure 10). The spectra were taken once when the electron beam covered the entire nanoparticle and also when only the edge of the nanoparticle was exposed to the focused electron beam. It can be seen that for the pristine nanoparticles both spectra (taken from the entire nanoparticle and its edge); (Figure 10a) consist of a broad hump between 6 and 11 eV and a main peak at 23.2 eV. These features are typical of bulk WS_2.[23] Nonetheless, the EELS spectrum from the nanoparticle edge is somewhat broader and asymmetric (Table 5) due to enhanced contribution of the surface plasmons.[24] The prominent peak at 23.2 eV is associated with the bulk plasmon excitation, involving the entire valence electron gas of the medium. The broad hump (centered around 8.5 eV) might be connected to the plasmon resonance which hybridizes with interband electron transitions.[23] The two corresponding spectra of the Rb intercalated particle, Figure 10b, are rather broad (Table 5) as compared to the spectra of the pristine particle, and the hump around 8.5 eV is washed out. The larger width of the plasmonic band in the intercalated particle may reflect lower homogeneity and may also be influenced by the rubidium single electron transitions associated with[25] the Rb($4p_{3/2}$) level at 15.2 eV and Rb ($4p_{1/2}$) at 16.1 eV.

XPS Characterization. Rubidium intercalated IF powder was characterized by X-ray photoelectron spectroscopy. The XPS measurements revealed that the elemental binding energies and the valence band of the intercalated sample shifted to higher energies by the same amount (600 mV) as compared to the pristine sample, Table 6. Elimination of charging was obtained by systematically varying the charging conditions from positive to negative values. These line shifts showed the same tendency as in our pervious work on intercalation of IF nanoparticles with sodium and potassium.[26] In contrast, the top of the valence band of the intercalated powder shifted by 200 mV only, Table 6, indicating the introduction of new (impurity) states into the

(23) Bell, M. G.; Liang, W. Y. *Adv. Phys.* **1976**, *25*, 53.
(24) Egerton, R. F. *Electron energy-loss spectroscopy in the electron microscope*, 2nd ed.; Plenum Press: New York, 1996.
(25) Ebbinghaus, G.; Simon, A. *Chem. Phys.* **1979**, *43*, 117.

forbidden gap. Figure 11a,b shows the W(4f) and S(2p) spectra of the intercalated and pristine powders. The shifts in binding energies of the intercalated IF powder to higher values are interpreted as an upward shift in the Fermi level, E_F; that is, the intercalated material becomes more electron rich than the pristine one. Note that both of the W(4f) and S(2p) bands of the intercalated material demonstrate a low binding energy shoulder (Figure 11a,b, arrows). These shoulders do not arise from differential charging, as proven by a systematic variation of the charging conditions (not shown). Thus, they are associated with a charge transfer (from the intercalant, Rb), where this extra charge remains relatively localized in the host lattice, for example, near defects like corners[27] and so forth.

On the basis of the XPS data only, it is difficult to estimate the atomic percentage of the intercalated rubidium. Clearly, part of the Rb signal corresponds to oxidized metal phase covering the surface of the nanoparticles. This fact was concluded from in situ chemically resolved electrical measurements (CREM).[28] By switching on the electron flood gun (eFG) to get a sample current of 60 nA, the W(4f) and S(2p) lines shifted by 50 mV (±0.15 mV) only, while the Rb(3d) line shifted by 310 mV (±0.15 mV). The CREM data (including additional eFG conditions, not shown) indicated that a major part of the detected Rb was situated externally to the nanoparticles, and yet was in direct contact with them (e.g., as an external coating). This Rb component was oxidized and was too dominant to allow the direct quntitative estimate of the intercalated Rb. In fact, the indirect information mentioned above, that is, the upward shift of the Fermi energy, was used as the evidence for the existence of the charge transfer from the guest (Rb atom) to the host WS_2 lattice. This charge transfer is believed to be the driving force for the intercalation process.[1]

Conclusions

IF-WS_2 nanoparticles and 2H-WS_2 (bulk) were subjected to the intercalation process with sodium, potassium, and rubidium. Special care was exerted to keep the intercalated phases in a moisture free environment during the study. The XRD analysis under the inert conditions showed that the intercalated material was inhomogeneous and was composed of several phases. The product was made up from intercalated and nonintercalated phases. Many of the nanoparticles were intercalated only at their outermost layers with the core remaining unchanged. Additionally Na_2S was formed in the course of the reaction of IF-WS_2 and sodium, and some potassium sulfide phases were also found in the intercalated nanoparticles. The van der Waals gap expansion of the intercalated particles depended on the radius of the alkali atom: the greatest interlayer expansion was obtained for the rubidium intercalation, the least for the intercalation with sodium atoms. The *a*-axis of the intercalated phase was found to expand as well. The fraction of the intercalated phases in the reacted (IF and 2H) powders depended on the specific alkali metal, with highest percentage of the intercalated phase achieved for rubidium intercalation in both kinds of powders. However, the amount of the intercalated IF phase was higher than the quantity of the intercalated 2H-WS_2 phase with the same metal under the same conditions. This observation could be associated with the difference in the surface to volume ratio of the two kinds of particles, which is greater by order of magnitude for the IF nanoparticles. The EELS analysis showed a broader plasmon line in the case of the rubidium intercalated particles. The XPS measurements of the rubidium intercalated IF-WS_2 powder revealed an upward shift in the Fermi level, E_F, corresponding to a guest-to-host electron transfer, and additionally indicated the existence of external coating on the nanoparticles, consisting of oxidized rubidium.

Acknowledgment. R.T. is the holder of the Drake family Chair in Nanotechnology and the Director of the Helen and Martin Kimmel Center for Nanoscale Science. This work was supported by "NanoMaterials, Ltd.", the GMJ Schmidt Minerva Center, the Harold Perlman Foundation, and the Israel Science Foundation.

CM800020P

(26) Feldman, Y.; Zak, A.; Tenne, R.; Cohen, H. *J. Vac. Sci. Technol., A* **2003**, *21*, 1752.
(27) Panich, A.; Kopnov, F.; Tenne, R. *J. Nanosci. Nanotechnol.* **2006**, *6*, 1.
(28) Cohen, H. *Appl. Phys. Lett.* **2004**, *85*, 1271.